Inorganic Chemistry

Article

First-Row Transition Metal Complexes of the Strongly Donating Pentadentate Ligand PY4Im

Jeremy M. Smith*,[†] and Jeffrey R. Long*,[‡]

[†]*Department of Chemistry and Biochemistry, MSC 3C, New Mexico State University, Las Cruces New Mexico 88003, United States, and [‡]Department of Chemistry, University of California, Berkeley, California 94720, United States*

The new ligand PY4Im, which incorporates an axial *N*-heterocyclic carbene and four equatorial pyridine donors, is readily prepared on a multigram scale. Six-coordinate first row transition metal complexes of the general formula $[(PY4Im)M(MeCN)]^{2+}$ (M = Fe, Co, Ni, Cu), where the PY4Im ligand coordinates in a square pyramidal pentadentate fashion, have been prepared. Structural, spectroscopic, and electrochemical characterization of these compounds provides evidence that PY4Im is a strongly donating ligand that favors the formation of low-spin complexes. Chemical oxidation of the iron(II) complex provides a low spin iron(III) complex, which has also been structurally and spectroscopically characterized. In the case of manganese(II), the PY4Im ligand is unable to either enforce a low-spin state or fully accommodate the metal ion. Rather, the ligand binds in a tridentate, face-capping mode.

Introduction

An axiom of coordination chemistry is that the design of supporting ligands is fundamental to controlling the properties of the metal center. For example, rigid pentadentate ligands that coordinate metals in a square pyramidal fashion are able to both enforce an octahedral geometry as well as restrict the metal substitution chemistry to a single coordination site. These properties are particularly important in controlling the reactivity of kinetically labile first row metals.

An archetypical pentadentate ligand is the polypyridyl $PY5H_2$ and its derivatives $PY5R_2$ (R = Me, OH, OMe; Figure 1). These ligands typically bind metal ions with one axial and four equatorial pyridine donors,[1,2] although other coordination modes are known.[1,3,4] The structural and electronic flexibility of the $PY5R_2$ family allows these ligands to coordinate a wide variety of transition metals, leading to their application in a number of areas, including the modeling of
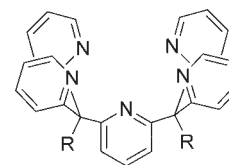
R = H, Me, OH, OMe

Figure 1. Pentadentate $PY5R_2$ ligands.

metalloenzyme active sites,[5] the construction of single-molecule magnets,[6,7] and water reduction electrocatalysis.[8]

A number of ligands share the structural framework of the $PY5R_2$ ligand but have different equatorial donor groups, and thus different stereoelectronic properties. For example, the pz_4lut ligand, in which the four equatorial donors are pyrazolyl groups, has a slightly stronger ligand field than the original $PY5H_2$ ligand.[9] Other related pentadentate ligands feature imidazole,[10] amine,[11] hydroxide,[12] and phosphine[13]

*To whom correspondence should be addressed. E-mail: jesmith@nmsu. edu (J.M.S.), jrlong@berkeley.edu (J.R.L.).

(1) de Vries, M. E.; La Crois, R. M.; Roelfes, G.; Kooijman, H.; Spek, A. L.; Hage, R.; Feringa, B. L. *Chem. Commun.* **1997**, 1549.
(2) Klein Gebbink, R. J. M.; Jonas, R. T.; Goldsmith, C. R.; Stack, T. D. P. *Inorg. Chem.* **2002**, *41*, 4633.
(3) Canty, A. J.; Minchin, N. J.; Skelton, B. W.; White, A. H. *J. Chem. Soc., Dalton Trans.* **1986**, 2205.
(4) Huang, J.-S.; Xie, J.; Kui, S. C. F.; Fang, G.-S.; Zhu, N.; Che, C.-M. *Inorg. Chem.* **2008**, *47*, 5727.
(5) (a) Jonas, R. T.; Stack, T. D. P. *J. Am. Chem. Soc.* **1997**, *119*, 8566. (b) Goldsmith, C. R.; Jonas, R. T.; Stack, T. D. P. *J. Am. Chem. Soc.* **2002**, *124*, 83. (c) Goldsmith, C. R.; Cole, A. P.; Stack, T. D. P. *J. Am. Chem. Soc.* **2005**, *127*, 9904. (d) Goldsmith, C. R.; Stack, T. D. P. *Inorg. Chem.* **2006**, *45*, 6048.

(6) (a) Freedman, D. E.; Jenkins, D. M.; Iavarone, A. T.; Long, J. R. *J. Am. Chem. Soc.* **2008**, *130*, 2884. (b) Freedman, D. E.; Jenkins, D. M.; Long, J. R. *Chem. Commun.* **2009**, 4829. (c) Bechlars, B.; D'Alessandro, D. M.; Jenkins, D. M.; Iavarone, A. T.; Glover, S. D.; Kubiak, C. P.; Long, J. R. *Nat. Chem.* **2010**, *2*, 362.
(7) Zadrozny, J. M.; Freedman, D. E.; Jenkins, D. M.; Harris, T. D.; Iavarone, A. T.; Mathonière, C.; Clérac, R.; Long, J. R. *Inorg. Chem.* **2010**, *49*, 8886.
(8) Karunadasa, H. I.; Chang, C. J.; Long, J. R. *Nature* **2010**, *464*, 1329.
(9) Morin, T. J.; Bennett, B.; Lindeman, S. V.; Gardinier, J. R. *Inorg. Chem.* **2008**, *47*, 7468.
(10) Tamagaki, S.; Kanamaru, Y.; Ueno, M.; Takagi, W. *Bull. Chem. Soc. Jpn.* **1991**, *64*, 165.

donors in the equatorial positions. Substitution of the axial pyridine by another donor is less common, but a pentadentate ligand with a central thiofuran unit flanked by four equatorial pyridine donors has been reported.[14]

Structurally analogous pentadentate ligands with increased ligand field strength may be expected to stabilize higher oxidation states.[15] More general interest in strongly donating ligands comes from the proposal that they may decrease the density of states in first row metal complexes and favor the two electron oxidation state changes typical of the second and third row metals.[16] One strategy for increasing the donor strength of pentadentate ligands is to replace one or more of the pyridines in PY5H$_2$ with an *N*-heterocyclic carbene (NHC) donor. Indeed, a large body of work has shown that NHCs are strong donors that bind covalently to a multitude of transition metals.[17] Moreover, multidentate ligands bearing NHC donors have been shown to stabilize high oxidation states.[18]

In this paper, we report the synthesis of a new strongly donating pentadentate ligand, PY4Im (1,3-bis(bis(2-pyridyl)methyl)imidazol-2-ylidene). The framework of this ligand is related to that of PY5H$_2$, with the axial pyridine replaced by an NHC donor. In addition, a series of first row transition metal complexes (Mn–Cu) supported by the PY4Im ligand has been prepared and characterized. The PY4Im ligand is found to be more strongly donating than PY5R$_2$ ligands, but with a binding pocket more suitable for smaller metal centers, a combination of properties that favors the formation of low-spin complexes.

Experimental Section

General Procedures. All transition metal complexes were prepared in a Vacuum Atmospheres glovebox. Bis(2-pyridyl)-bromomethane was prepared by a literature procedure,[19] using benzene instead of CCl$_4$ as the solvent and recrystallized from CH$_2$Cl$_2$/Et$_2$O at −25 °C. Thianthrenyl hexafluorophosphate was prepared similarly to a literature procedure[20] and stored

at −25 °C. Acetonitrile, diethyl ether, toluene, and tetrahydrofuran were purified by a Vacuum Atmospheres solvent purification system. All other reagents were obtained from commercial vendors and used without further purification.

Spectroscopic Measurements. Cyclic voltammograms were obtained with a Bioanalytical Systems CV-50W voltammetric analyzer, a platinum wire counter electrode, a silver wire reference electrode, and a platinum disk working electrode. Analyte solutions (ca. 1 mM in metal complex) were prepared with 0.1 M NBu$_4$PF$_6$ in MeCN. Ferrocene was used as an internal standard. All potentials are referenced to the Cp$_2$Fe/Cp$_2$Fe$^+$ couple.

^{1}H (400.13 MHz) NMR spectra were collected using Bruker AVB-400 or AVQ-400 spectrometers, while ^{19}F (376.50 MHz) and ^{31}P{^{1}H} (161.97 MHz) NMR spectra were collected using a Bruker AVQ-400 spectrometer. Resonances in the ^{1}H NMR spectra are referenced to residual CD$_2$HCN (1.94 ppm) and CHCl$_3$ (7.26 ppm). Resonances in the ^{19}F and ^{31}P NMR spectra are referenced to external CFCl$_3$ (0.0 ppm) and trimethyl phosphate (3.0 ppm), respectively. Solution magnetic susceptibilities were determined by the Evans' method.[21]

Frozen solution electron paramagnetic resonance (EPR) spectra were collected in methanol at 9.25 GHz (X-band) frequency at 8 K using a Varian E-109 spectrometer equipped with an E-102 microwave bridge. The temperature was controlled by an Air Products Heli-tran liquid helium cryostat. Data were collected with 100 kHz magnetic field modulation and 32 G modulation amplitude. The microwave frequency was calibrated using a standard sample of DPPH (2,2-diphenyl-1-picrylhydrazyl).

Solution UV−vis spectra were collected using a CARY 5000 spectrophotometer interfaced with Varian UV−vis software. Infrared spectra were obtained on a Perkin-Elmer Spectrum 100 Optica FTIR spectrometer. Elemental analyses were performed at the Microanalytical Laboratory of the University of California, Berkeley.

Synthesis of Compounds. **[PY4ImH]Br (1).** A solution of NaOH (764 mg, 19.1 mmol) and imidazole (1.30 g, 19.1 mmol) in H$_2$O (8 mL) and MeCN (20 mL) was stirred at room temperature (RT) for 20 min. Bis(2-pyridyl)bromomethane (5.00 g, 20.1 mmol) was added to the solution, and the reaction heated at reflux overnight. After cooling, a second portion of bis(2-pyridyl)-bromomethane (5.00 g, 20.1 mmol) was added, and the reaction was again heated at reflux overnight. The reaction mixture was cooled to RT, and the solvent removed by rotary evaporation. Water (20 mL) and CH$_2$Cl$_2$ (100 mL) were added to the residue. The layers were separated, and the aqueous layer extracted with CH$_2$Cl$_2$ (3 × 20 mL). The combined organic layers were dried (MgSO$_4$) and filtered. The solution was concentrated to about 50 mL and layered with Et$_2$O (30 mL). Cooling to −25 °C led to the crystallization of an off-white solid that was sufficiently pure for further use (8.03 g, 87%). ^{1}H NMR (400 MHz, CDCl$_3$, 22 °C) δ 10.45 (s, 1H, Im-H); 8.52 (d, J_{HH} = 6 Hz, 4 H, py-H); 7.99 (s, 2 H, Im-H); 7.78 (s, 2 H, C−H); 7.71−7.63 (m, 8 H, py-H); 7.26−7.20 (m, 4H, py-H).

[PY4ImH](CF$_3$SO$_3$) (2). A slurry of KCF$_3$SO$_3$ (230 mg, 1.22 mmol) in MeCN (5 mL) was added to PY4ImHBr (500 mg, 1.03 mmol) in MeCN (5 mL). After stirring for 30 min, the white solid (KBr) was removed by filtration. The solvent was removed by rotary evaporation to yield a colorless solid (563 mg, 98%). Crystals suitable for X-ray diffraction were grown by vapor diffusion of Et$_2$O into a MeCN solution. ^{1}H NMR (400 MHz, CDCl$_3$, 22 °C) δ 9.98 (s, 1 H, Im-H); 8.59 (d, J_{HH} = 5 Hz, 4 H, py-H); 7.90 (s, 2 H, Im-H); 7.77−7.73 (dt, J_{HH} = 8 Hz, J_{HH} = 2 Hz, 4 H, py-H); 7.59 (d, 8 Hz, 4 H, py-H); 7.31−7.29 (m, 4 H, py-H); 7.26 (s, 2 H, C−H). ^{19}F NMR (CDCl$_3$, 22 °C) −78.3

(11) (a) Grohmann, A.; Knoch, F. *Inorg. Chem.* **1996**, *35*, 7932. (b) Grohmann, A.; Knoch, F. *Dalton Trans.* **2010**, *39*, 1432 and references cited therein.

(12) Schmidt, S.; Omnès, L.; Heinemann, F. W.; Kuhnigk, J.; Krüger, C.; Grohmann, A. *Z. Naturforsch. B* **1998**, *53*, 946.

(13) (a) Zimmermann, C.; Heinemann, F. W.; Grohmann, A. *Eur. J. Inorg. Chem.* **2005**, 3506. (b) Kohl, S. W.; Heinemann, F. W.; Hummert, M.; Weißhoff, H.; Grohmann, A. *Eur. J. Inorg. Chem.* **2006**, 3901. (c) Kohl, S. W.; Heinemann, F. W.; Hummert, M.; Bauer, W.; Grohmann, A. *Chem.—Eur. J.* **2006**, *4*, 4313.

(14) Fazio, O.; Gnida, M.; Meyer-Klaucke, W.; Frank, W.; Kläui, W. *Eur. J. Inorg. Chem.* **2002**, 2891.

(15) Pitarch López, J.; Heinemann, F. W.; Prakash, R.; Hess, B. A.; Horner, O.; Jeandey, C.; Oddou, J.-L.; Latour, J.-M.; Grohmann, A. *Chem.—Eur. J.* **2002**, *8*, 5709.

(16) Volpe, E. C.; Wolczanski, P. T.; Lobkovsky, E. B. *Organometallics* **2010**, *29*, 364.

(17) Selected reviews: (a) Diéz-González, S.; Nolan, S. P. *Coord. Chem. Rev.* **2007**, *251*, 874. (b) de Frémont, P.; Marion, N.; Nolan, S. P. *Coord. Chem. Rev.* **2009**, *253*, 862.

(18) (a) Forshaw, A. P.; Bontchev, R. P.; Smith, J. M. *Inorg. Chem.* **2007**, *46*, 3792. (b) Nieto, I.; Ding, F.; Bontchev, R. P.; Wang, H.; Smith, J. M. *J. Am. Chem. Soc.* **2008**, *130*, 2716. (c) Vogel, C.; Heinemann, F. W.; Sutter, J.; Anthon, C.; Meyer, K. *Angew. Chem., Int. Ed.* **2008**, *47*, 2681. (d) Scepaniak, J. J.; Fulton, M. D.; Bontchev, R. P.; Duesler, E. N.; Kirk, M. L.; Smith, J. M. *J. Am. Chem. Soc.* **2008**, *130*, 10515. (e) Scepaniak, J. J.; Young, J. A.; Bontchev, R. P.; Smith, J. M. *Angew. Chem., Int. Ed.* **2009**, *48*, 3158.

(19) Vedernikov, A. N.; Fettinger, J. C.; Mohr, F. *J. Am. Chem. Soc.* **2004**, *126*, 11160.

(20) Shine, H. J.; Zhao, B.-J.; Marx, J. N.; Ould-Ely, T.; Whitmire, K. H. *J. Org. Chem.* **2004**, *69*, 9255.

(21) Baker, M. V.; Field, L. D.; Hambley, T. W. *Inorg. Chem.* **1988**, *27*, 2872.

($OSO_2CF_3{}^-$): Anal. Calcd for $C_{26}H_{21}F_3N_6O_3S$ C 56.31, H 3.82, N 15.15. Found C 56.33, H 3.70, N 15.10.

(PY4Im)AgBr (3). A 50 mL round-bottom flask was charged with Ag_2O (1.19 g, 5.15 mmol), [PY4ImH]Br (5.00 g, 10.3 mmol), and CH_2Cl_2 (25 mL). The reaction mixture was stirred at RT for 6 h. The resulting off-white solid was isolated by filtration, washed with Et_2O, and dried under vacuum. The supernatant was layered with Et_2O (25 mL) and cooled to −25 °C. Additional product crystallized overnight as a gray solid. Total yield 4.96 g (81%). Small amounts of colored impurities were removed by recrystallization from chloroform. ^{1}H NMR (400 MHz, $CDCl_3$, 22 °C) δ 8.59 (d, $J_{HH} = 4$ Hz, 4 H, py-H); 7.71 (dt, $J_{HH} = 10$ Hz, $J_{HH} = 2$ Hz, 4H, py-H); 7.50 (s, 2 H, Im-H); 7.31−7.23 (m, 8H, py-H); 7.01 (s, 2H, C−H). Anal. Calcd. for $C_{25}H_{20}AgBrN_6 \cdot 2.5CHCl_3$: C 37.08, H 2.55, N 9.44. Found C 36.88, H 2.42, N 9.77.

[(PY4Im)Fe(MeCN)](PF$_6$)$_2$ (4). A 20 mL scintillation vial was charged with (PY4Im)AgBr (150 mg, 253 μmol), FeI_2 (78 mg, 253 μmol) and MeCN (6 mL). The resulting red-orange slurry was stirred overnight. A solution of $TlPF_6$ (177 mg, 506 μmol) in MeCN (2 mL) was added to the reaction mixture, leading to dissolution of the red solid. After stirring for 30 min, the reaction mixture was filtered to yield a red solution. The solution was layered over toluene (8 mL) and stored at RT. The air-stable product crystallized as red blocks (199 mg, 99% yield). ^{1}H NMR (400 MHz, CD_3CN, 22 °C) δ 9.41 (d, $J_{HH} = 6$ Hz, 4H, py-H); 7.95 (s, 2 H, Im-H); 7.80−7.75 (m, 8 H, py-H); 7.33−7.31 (m, 4 H, py-H); 7.23 (s, 2H, C−H); ^{19}F NMR (CD_3CN, 22 °C) δ −72.0 (d, $J_{PF} = 707$ Hz) $PF_6{}^-$; [31]P{[1]H} (CD_3CN, 22 °C) δ −144.6 (septet, $J_{PF} = 707$ Hz) $PF_6{}^-$. UV−vis (MeCN) λ_{max} (ε_M, $M^{-1} \cdot cm^{-1}$) 459 (7990), 400 (6564), 361 (4534). Anal.Calcd for $C_{28}H_{23}F_{12}FeN_6P_2 \cdot C_7H_8$: C 46.22, H 3.54, N 11.10. Found C 46.86, H 3.76, N 11.02.

General Procedure for the Synthesis of [(PY4Im)M(MeCN)] (CF$_3$SO$_3$)$_2$ (M = Co, Ni, Cu, 5−7). A 20 mL scintillation vial was charged with (PY4Im)AgBr (100 mg, 169 μmol), $M(CF_3SO_3)_2$ (169 μmol), and MeCN (8 mL). The reaction was stirred overnight at RT (in the case of copper, prolonged stirring resulted in decomposition of the product). The AgBr byproduct was removed by vacuum filtration, and the product crystallized by vapor diffusion of Et_2O into MeCN. Characterization data for these complexes is listed below.

[(PY4Im)Co(MeCN)](CF$_3$SO$_3$)$_2$ (5). Slightly air-sensitive orange-red solid (108 mg, 80%). ^{1}H NMR (400 MHz, CD_3CN, 22 °C) δ 20.5, 12.6, 9.4, 8.0, 3.4, 1.1. ^{19}F NMR (CD_3CN, 22 °C) −78.1 ($OSO_2CF_3{}^-$). μ_{eff} (Evans') = 1.7(1) μ_B. UV−vis (MeCN): λ_{max} (ε_M, $M^{-1} \cdot cm^{-1}$) 842 (sh, 63), 679 (103), 610 (110), 380 (4500), 353 (4113), 319 (sh, 4159). IR (ATR): ν (cm^{-1}) 3140, 1648, 1602, 1473, 1443, 1249, 1224, 1155, 1028, 765, 704, 614, 573, 516. Anal. Calcd for $C_{30}H_{23}F_6N_6CoO_6S_2 \cdot C_4H_{10}O$: C 45.21, H 3.79, N 11.18. Found C 44.86, H 3.39, N 11.60.

[(PY4Im)Ni(MeCN)](CF$_3$SO$_3$)$_2$ (6). Air-stable orange solid (124 mg, 92%). ^{1}H NMR (400 MHz, CD_3CN, 22 °C) δ 66 (s, 2H, Im-H/C−H); 53 (s, 4H, py-H); 44 (s, 4H, py-H); 14 (s, 4H, py-H); 2 (s, 4H, py-H); −14 (s, 2H, Im-H/C−H); ^{19}F NMR (CD_3CN, 22 °C) −78.3 ($OSO_2CF_3{}^-$). μ_{eff} (Evans') = 2.9(1) μ_B. UV−vis (MeCN): λ_{max} (ε_M, $M^{-1} \cdot cm^{-1}$) 757 (46), 535 (35), 370 (699), 303 (834). IR (ATR): ν (cm^{-1}) 3130, 2981, 1601, 1473, 1444, 1252, 1223, 1159, 1028, 1015, 860, 767, 660, 636, 611, 573, 516. Anal. Calcd for $C_{30}H_{23}F_6N_6NiO_6S_2$: C 43.41, H 2.89, N 12.22. Found C 43.61, H 3.05, N 11.93.

[(PY4Im)Cu(MeCN)](CF$_3$SO$_3$)$_2$ (7). Air-stable purple solid (79 mg, 58%). μ_{eff} (Evans') = 1.7(3) μ_B UV−vis (MeCN): λ_{max} (ε_M, $M^{-1} cm^{-1}$) 742 (sh, 392), 544 (1377), 334 (sh, 5071). IR (ATR): ν (cm^{-1}) 3128, 1602, 1592, 1473, 1442, 1243, 1225, 1151, 1004, 860, 774, 763, 736, 690, 661, 636, 573, 516. Anal. Calcd for $C_{27}H_{20}CuF_6N_6O_6S_2$: C 42.33, H 2.63, N 10.97. Found C 42.19, H 2.63, N 10.97.

[(PY4Im)Fe(MeCN)](PF$_6$)$_3$ (8). Solid thianthrenyl hexafluorophosphate (46 mg, 130 μmol) was added to a red solution of [(PY4Im)Fe(MeCN)](PF$_6$)$_2$ (100 mg, 130 μmol) in MeCN (5 mL). The resulting dark purple solution was stirred overnight at RT. The solution was filtered and layered over toluene (5 mL) and stored at RT. The product was obtained as moisture-sensitive red needles (110 mg, 90% yield). ^{1}H NMR (400 MHz, CD_3CN, 22 °C) δ 46 (s, 2H, Im-H/C−H); 28 (s, 3H, MeCN); 13 (s, 4H, py-H); 9 (s, 4H, py-H); 3 (s, 4H, py-H); −51 (s, 4H, py-H); −61 (s, 2H, Im-H/C−H); ^{19}F NMR (CD_3CN, 22 °C) δ −72.0 (d, $J_{PF} = 707$ Hz) $PF_6{}^-$; [31]P{[1]H} (CD_3CN, 22 °C) δ −144.6 (septet, $J_{PF} = 707$ Hz) $PF_6{}^-$. μ_{eff} (Evans') = 2.5(1) μ_B. UV−vis (MeCN): λ_{max} (ε_M, $M^{-1} \cdot cm^{-1}$) 528 (sh, 74), 408 (sh, 669). IR (ATR): ν (cm^{-1}) 3101, 3014, 2981, 2947, 1612, 1475, 1449, 1377, 1351, 1323, 1251, 1163, 1028, 800, 335, 716, 661, 654, 623, 555. Anal. Calcd for $C_{28}H_{23}F_{18}FeN_6P_3 \cdot 2MeCN \cdot C_7H_8$: C 41.10, H 3.36, 11.35. Found C 41.08, H 3.39, N 11.76.

[(κ^3-PY4Im)Mn(MeCN)$_3$](PF$_6$)$_2$ (9). A 20 mL scintillation vial was charged with (PY4Im)AgBr (200 mg, 340 μmol), $MnCl_2$ (42 mg, 340 μmol), and MeCN (4 mL). The reaction was stirred overnight at RT. A solution of $TlPF_6$ (240 mg, 680 μmol) in MeCN (2 mL) was added to the reaction mixture. After stirring for 30 min, the reaction was filtered to yield a pale yellow-orange solution. The colorless product was crystallized by diffusion of Et_2O into MeCN (170 mg, 57%). Colorless solutions of the complex slowly develop a yellow coloration when exposed to air. ^{19}F NMR (CD_3CN, 22 °C) δ −70.0 (d, $J_{PF} = 707$ Hz) $PF_6{}^-$; [31]P{[1]H} (CD_3CN, 22 °C) δ −143.9 (septet, $J_{PF} = 707$ Hz) $PF_6{}^-$. μ_{eff} (Evans') = 5.4(2) μ_B. IR (ATR) ν (cm^{-1}) 2587, 3159, 2272, 2255, 1599, 1591, 1475, 1437, 1410, 1146, 1016, 800, 768, 752, 675, 667, 6238, 615, 555, 534. Anal. Calcd for $C_{31}H_{29}F_{12}MnN_9P_2$: C 42.67, H 3.35, N 14.45. Found C 42.68, H 3.23, N 14.50.

X-ray Structure Determinations. Structures were determined for compounds **2−9**. X-ray diffraction analyses were performed on single crystals coated with Paratone-N oil and mounted on Kaptan loops. The crystals were frozen under a stream of N_2 during measurements. Data were collected using either a Bruker X8 APEX diffractometer equipped with a Bruker MICRO-STAR X-ray source, APEX-II detector, and a Cu anode (λ = 1.5406 Å) or a Bruker SMART diffractometer equipped with an APEX detector using MoKα (λ = 0.71073 Å) radiation. Raw data were integrated and corrected for Lorentz and polarization effects using Bruker APEX2 v. 2009.1.[22] Absorption corrections were applied using SADABS.[23] Space group assignments were determined by the examination of systematic absences, E-statistics, and successive refinement of the structures. Crystal structures were solved by direct methods using SIR-92.[24] None of the crystals showed significant decay during data collection. Thermal parameters were refined for all non-hydrogen atoms. Hydrogen atoms were placed in ideal positions and refined using a riding model for all structures. Disorder of $PF_6{}^-$ was modeled with the use of free variables. Solvent disorder was extensive and impossible to model in **8**, and SQUEEZE[25] was used to account for unassigned electron density.

Results and Discussion

The pentadentate ligand PY4Im is conceptually related to PY5R$_2$ pentapyridine ligands,[1,1,3,7] with the axial pyridine in these ligands replaced by an imidazol-2-ylidene-based N-heterocyclic carbene donor (Figure 2). Thus, the PY4Im ligand is

(22) *APEX2*, v.2009; Bruker Analytical X-Ray Systems, Inc: Madison, WI, 2009.

(23) Sheldrick, G. M. *SADABS*, Version 2.03; Bruker Analytical X-Ray Systems, Inc: Madison, WI, 2000.

(24) Altomare, A.; Cascarano, G.; Giacovazzo, C.; Guagliardi, A. *J. Appl. Crystallogr.* **1993**, *26*, 343.

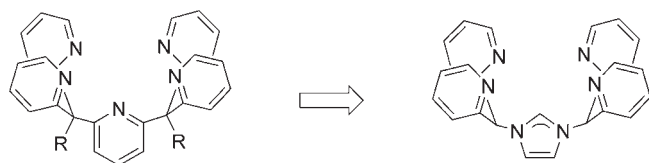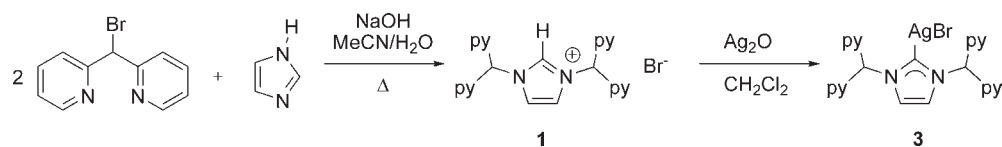(25) van der Sluis, P.; Spek, A. L. *Acta Crystallogr.* **1990**, *46*, 194.
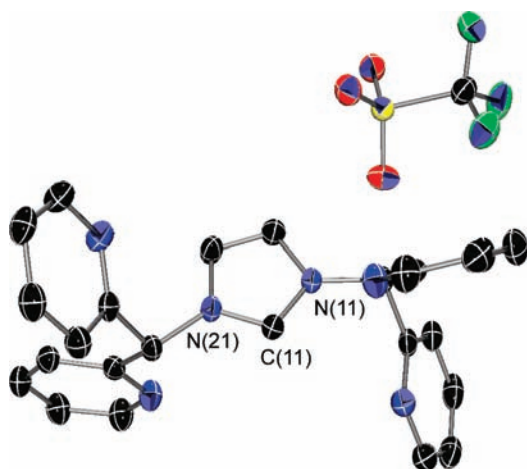
Scheme 1

Figure 2. Conceptual relationship between PY5R$_2$ and PY4Im ligands.

Figure 3. X-ray crystal structure of [PY4ImH](CF$_3$SO$_3$) **2**. Thermal ellipsoids are shown at 50% probability; hydrogen atoms are omitted for clarity. Selected bond lengths (Å) and angles (deg): N(21)−C(11) 1.329(2); N(11)−C(11) 1.327(2); N(11)−C(11)−N(21) 108.0(1).

composed of two bis(2-pyridyl) arms that flank a central NHC donor. In principle, the modularity of the ligand design allows for variants with other donor groups to be prepared.

Multigram quantities of the PY4Im ligand can be prepared from imidazole via a short synthetic route. In a one-pot synthesis, the imidazolium salt [PY4ImH]Br **1** is assembled in a similar method to that used for the synthesis of 1,3-dibenzhydrylbenzimidazolium bromide.[26] Thus, deprotonated imidazole is heated with 2 equiv of Py$_2$CHBr,[19] added sequentially in two portions, affording **1** in high yield (Scheme 1).

Single crystals of the imidazolium cation were obtained as the triflate salt, [PY4ImH](CF$_3$SO$_3$) (**2**), following anion exchange with KCF$_3$SO$_3$ (Figure 3). The X-ray crystal structure of **2** shows the expected 1,3-disubstituted imidazolium salt. There are no unusual bond lengths and angles in the structure, and in particular the N(21)−C(11) and N(11)−C(11) bond distances and N(11)−C(11)−N(21) bond angle are typical of imidazolium salts.

Initial attempts to generate the *N*-heterocyclic carbene by deprotonation of **1** with strong bases such as KO^{t}Bu and LDA resulted in intractable mixtures of products. However, as with the synthesis of many imidazol-2-ylidene ligands,[27]

(26) Huynh, H. V.; Wong, L. R.; Ng, P. S. *Organometallics* **2008**, *27*, 2231.
(27) Lin, I. J. B.; Vasam, C. S. *Coord. Chem. Rev.* **2007**, *251*, 642.

deprotonation of [PY4ImH]Br with Ag$_2$O leads to the ligand transfer reagent (PY4Im)AgBr **3** in high yield and under mild conditions (Scheme 1).

Single crystal X-ray analysis reveals that **3** forms a tetramer in the solid state (Figure 4). The central portion of the structure consists of a (AgBr)$_4$ core that adopts a chair conformation and is surrounded by four PY4Im ligands. The (AgBr)$_4$ core is in turn composed of two (AgBr)$_2$ dimers that are related by a crystallographic inversion center. Both silver ions in the (AgBr)$_2$ dimers are four-coordinate, but have different first coordination spheres. One silver ion (Ag(1)) is bound to a monodentate PY4Im ligand (Ag(1)−C(1A) = 2.150(3) Å) and two bridging bromide ligands (Ag(1)−Br(1)=2.6409(5) Å, Ag(1)−Br(2)=2.7126(5) Å). The coordination sphere is completed by a relatively long bond to one of the pyridine donors from a bridging PY4Im ligand (Ag(1)−N(3B) = 2.586(2) Å). The second silver ion (Ag(2)) is bound to the carbene donor (Ag(2)−C(1B) = 2.145(2) Å) of the bridging PY4Im ligand and the two bridging bromide ligands (Ag(2)−Br(1) 2.7469(6) Å, Ag(2)−Br(2) 2.7513(6) Å). The coordination sphere of Ag(2) is completed by the Ag(2)−Br(2)′ bond (2.7923(6) Å) which also bridges the two (AgBr)$_2$ dimers. Thus, there are two types of PY4Im ligand in the solid state structure of (PY4Im)AgBr: one is monodentate, coordinating to one silver ion through the NHC carbon, while the second is bidentate, coordinating to the same silver ion through one of the pyridine donors and to a second silver ion through the NHC carbon. The bridging bidentate bonding mode of the second PY4Im ligand also helps bridge the two (AgBr)$_2$ units. The central NHC donors of both PY4Im ligands show similar structural features. As with other NHC ligands, there is a slight lengthening of the C−N bonds and a decrease in the NCN angles upon formation of the carbene.

In contrast to the low symmetry solid-state structure, **3** exhibits C_{2v} symmetry in solution, as determined by ^{1}H NMR spectroscopy. Thus, only a single set of resonances is observed for the imidazol-2-ylidene and methine protons, which resonate as singlets at 7.50 ppm and 7.01 ppm, respectively. Furthermore, there are only four sets of resonances arising from the pyridine ring protons. The low solubility of this complex in common organic solvents has precluded a satisfactory ^{13}C{^{1}H} NMR spectrum.

The silver complex **3** serves as a mild reagent for transferring the PY4Im ligand to first row transition metals. Thus, in the presence of non-coordinating anions (e.g., CF$_3$SO$_3^-$, PF$_6^-$), reaction of **3** with suitable divalent metal salts (i.e., iron to copper) results in good to excellent yields of ionic complexes having the general formula [(PY4Im)M(MeCN)]$^{2+}$ (**4**−**7**) (Schemes 2 and 3). The structures of all these complexes have been determined by X-ray crystallography,[28] with selected metrical parameters enumerated in Table 1. The combined structural and spectral characterization show that the PY4Im

(28) See Supporting Information for full details.
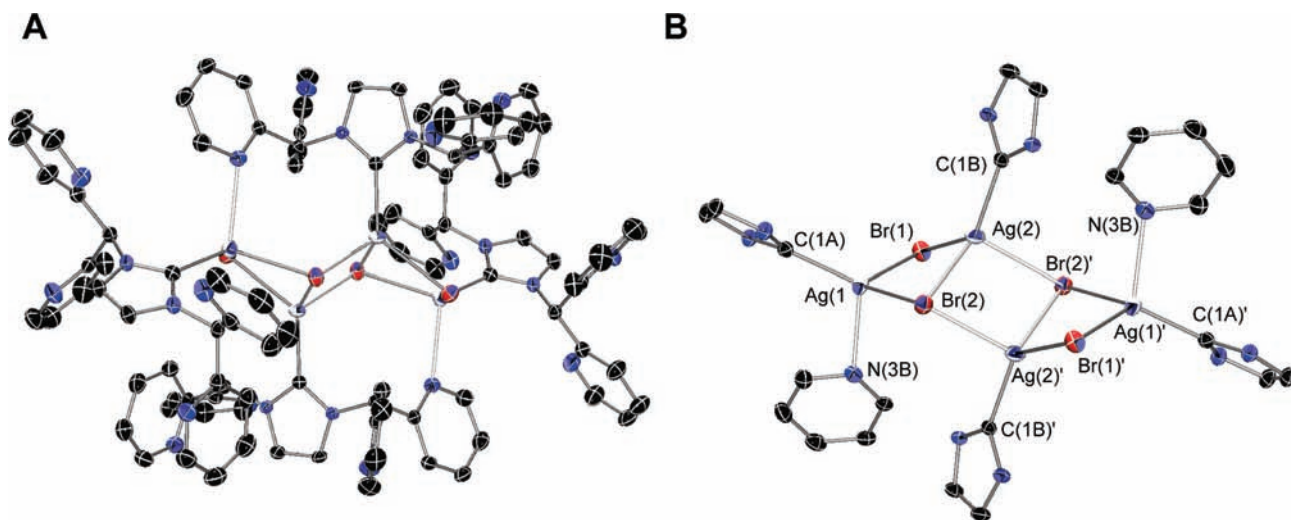
Figure 4. (**A**) X-ray crystal structure of (PY4Im)AgBr **3**. Thermal ellipsoids are shown at 50% probability; hydrogen atoms and solvent molecules omitted for clarity. (**B**) Close up of (PY4Im)AgBr, showing the eight-membered $(AgBr)_4$ core. Selected bond lengths (Å) and angles (deg): Ag(1)−C(1A) 2.150(3); Ag(1)−Br(1) 2.6409(5); Ag(1)−Br(2) 2.7126(5); Ag(1)−N(3B) = 2.586(2); Ag(2)−C(1B) = 2.145(2); Ag(2)−Br(1) 2.7469(6), Ag(2)−Br(2) 2.7513(6); Ag(2)−Br(2)′ 2.7923(6); C(1A)−N(2A) 1.354(3); C(1A)−N(1A) 1.357(3); C(1B)−N(2B) 1.352(3); C(1B)−N(1B) 1.355(3); N(2A)−C(1A)−N(1A) 103.8(2); N(2B)−C(1B)−N(1B) 103.9(2).

Scheme 2

M = Co (**4**), Ni (**5**), Cu (**6**)
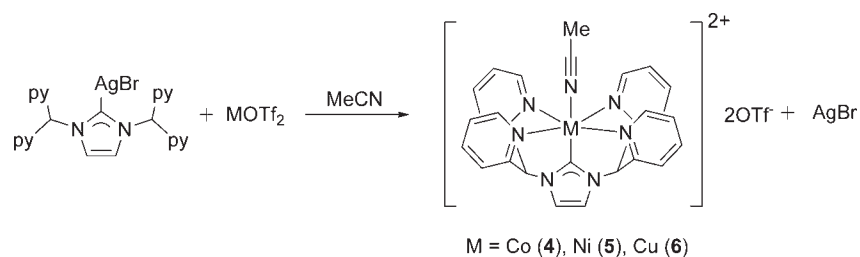
Scheme 3
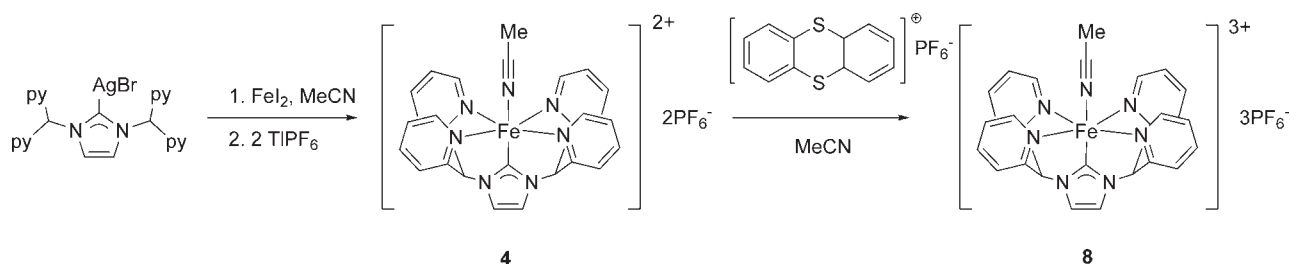
ligand has strong a tendency to stabilize six-coordinate complexes with low-spin electronic configurations (see below).

As exemplified by the structure of [(PY4Im)Fe(MeCN)] $(CF_3SO_3)_2$, **4**, all of these complexes are six- coordinate in the solid state: five of the coordination sites are occupied by the pentadentate PY4Im ligand and the sixth by acetonitrile (Figure 5). The most notable structural feature common to all of the complexes is the short M−C(11) bond of about 1.9 Å, which shows little change across the series. For complexes **4**, **5**, and **6**, this M−NHC bond distance is the shortest known in six-coordinate complexes of these metals. Interestingly, there is also very little change in the M−NCMe bond lengths across the series. All other metal−ligand bond lengths are within normal ranges, with the exception of cobalt and copper, where the addition of electrons into antibonding

orbitals has the greatest effect on the equatorial M−py bond lengths.

In the case of the cobalt and copper derivatives **5** and **7**, significant elongation of two *trans* M−N bonds in the Py4 plane is observed. For example, in **5**, the Co−N(12) and Co−N(15) bonds are over 0.1 Å longer than the Co−N(13) and Co−N(14) bonds (Table 1), which is attributed to a Jahn−Teller distortion in this low spin d^7 complex. A similar distortion is observed in the structure of **7**; in this case the bond length difference is over 0.2 Å. A similar elongation of two *trans* donor metal ligand bonds has been observed in the related complex $[(pz_4lut)CuCl]^+$.[9]

Given the topological similarities of the PY4Im and $PY5R_2$ ligands, it is not surprising that related trends are observed in the structural data of their metal complexes. For

Table 1. Selected Distances (Å) and Angles (deg) for [(PY4Im)M(MeCN)]$^{2+}$ Complexes in **4−7**
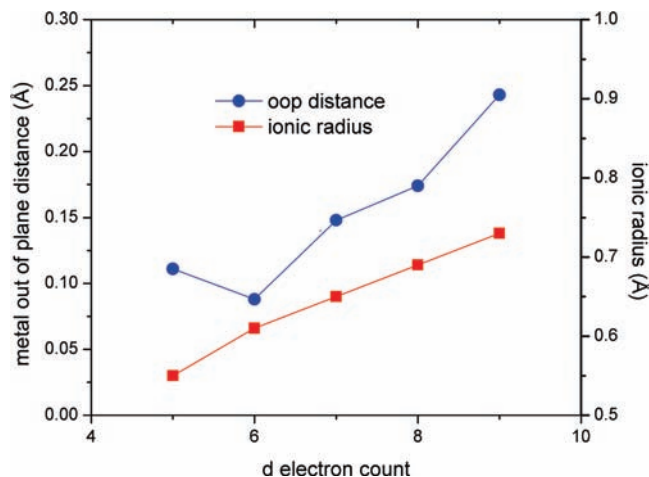
bond distance/angle	**4** (Fe)	**5** (Co)	**6** (Ni)	**7** (Cu)
M−C11	1.849(2)	1.845(6)	1.919(3)	1.889(4)
M−N12	2.022(2)	2.214(5)	2.184(3)	2.390(4)
M−N13	2.013(2)	2.056(5)	2.191(3)	2.144(4)
M−N14	2.015(2)	2.073(5)	2.174(3)	2.146(3)
M−N15	2.023(2)	2.238(5)	2.172(3)	2.459(4)
M−py(ave)	2.018(2)	2.145(5)	2.181(3)	2.284(4)
M−N16	1.981(2)	1.958(5)	2.038(3)	1.961(4)
M oop^a	0.0884(8)	0.148(3)	0.174(1)	0.243(2)
C11−M−N16	177.81(7)	179.3(2)	179.0(1)	177.3(2)
N12−M−N15	173.78(6)	171.7(2)	169.9(1)	165.6(1)
N13−M−N14	176.08(5)	172.5(2)	171.8(1)	170.0(1)
NHC tilt^b	88.44(6)	89.6(2)	88.7(1)	89.4(2)

^{a} Displacement of the metal center from the plane defined by the four equatorial pyridines. ^{b} Angle between the least-squares plane of the NHC group and the least-squares plane defined by the four equatorial pyridines.
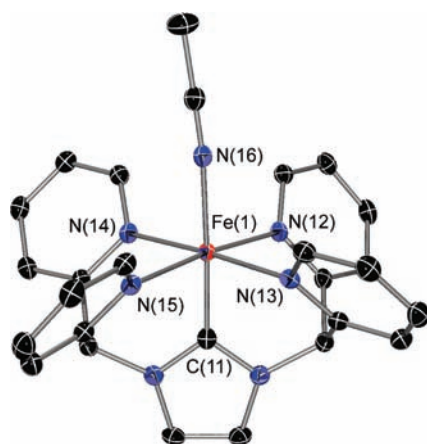
Figure 5. X-ray crystal structure of [(PY4Im)Fe(MeCN)]$^{2+}$ in **4**, showing the atomic labeling scheme. Thermal ellipsoids are shown at 50% probability; hexafluorophosphate anions, solvent molecules, and hydrogen atoms are omitted for clarity.

Figure 6. Plots of displacement of metal ion from the equatorial Py4 plane as a function of d electron count for [(PY4Im)M(MeCN)]$^{2+/3+}$ complexes (●) and six-coordinate, low-spin ionic radius as a function of d electron count (■).

all four of the divalent transition metal complexes, the metal ion in the PY4Im complexes resides slightly above the plane defined by the pyridine donors (Table 1). This out-of-plane distance increases from iron to copper, and follows the change in ionic radius of the low-spin metal ion (Figure 6).[29] Interestingly, this trend is opposite to that observed for the PY5 (OMe)$_2$ ligand,[1] which has a greater proclivity for stabilizing high-spin electronic states. The smallest out-of-plane displacement is observed for complex **4**, suggesting that low-spin iron(II) has the best match for the ligand binding pocket. Indeed, the bond angles in the iron(II) complex **4** show the smallest distortion from ideal octahedral geometry at the metal center. Since low-spin ions are smaller than their high-spin congeners, the metal ion that has the best fit for PY4Im is smaller than that for PY5R$_2$ or pz$_4$lut.[9]

In contrast to the related PY5R$_2$ complexes,[1] but similarly to pz$_4$lut complexes,[9] the imidazolylidene ring of the axial NHC donor is perpendicular to the plane of the four pyridine rings. The average M−N−C−C(sp^3) torsion is intermediate between that measured for PY5R$_2$ and pz$_4$lut complexes, for example, in the case of nickel(II) complexes,[9] the average torsion angle is 9.8° for PY5OMe$_2$, 1.8° for pz$_4$lut and 4.8° for PY4Im.[28]

(29) Shannon, R. D. *Acta Crystallogr.* **1976**, *A32*, 751.

The solution ^{1}H NMR spectra of complexes **4** and **6** are consistent with the solid-state structures. For the diamagnetic iron complex **4**, the imidazol-2-ylidene backbone protons resonate as a singlet at 7.95 ppm, as do the methine protons at 7.23 ppm. Four sets of resonances are observed for the pyridine protons, a doublet at 9.41 ppm, two sets of multiplets between 7.80 and 7.75 ppm, and a multiplet between 7.33 and 7.31 ppm. The ^{1}H NMR spectrum of the nickel complex in **6** gives six paramagnetically shifted resonances with appropriate relative integrations for the PY4Im ligand. The solution magnetic moments of the paramagnetic complexes were determined by the Evans′ method, providing spin states of $S = \frac{1}{2}$ (**5**), $S = 1$ (**6**), and $S = \frac{1}{2}$ (**7**).

Although no EPR spectra were observed at RT in fluid solution, frozen solution EPR spectra (MeOH, 10 K) were observed for the two $S = \frac{1}{2}$ complexes **5** and **7**. The EPR spectrum of complex **5** has apparent axial symmetry, with $g_\perp \approx 2.21$ and $g_\parallel \approx 2.11$, consistent with low-spin cobalt(II).[28] The EPR spectrum of **7** also has apparent axial symmetry, with $g_\perp \approx 2.23$ and $g_\parallel \approx 2.08$. While hyperfine coupling was evident in the EPR spectra of both complexes, the spectra could not be satisfactorily simulated because of the relatively large linewidths.

The electronic spectra for compounds **4−7** are dominated by intense charge-transfer bands that obscure the ligand-field transitions. Only in the case of the nickel(II) complex in **6** can the d-d transitions be assigned. Considering the geometry to be approximately octahedral provides $\Delta_o = 13333$ cm^{-1} from the lowest energy transition at 750 nm, which is larger than that measured for [(PY5Me$_2$)Ni(MeCN)]$^{2+}$ ($\Delta_o = 12594$ cm^{-1}).[7]

The cyclic voltammograms of compounds **4−6** in acetonitrile all show a reversible wave that is ascribed to the [(PY4Im)M(MeCN)]$^{2+/3+}$ couple (Table 2). There is no evidence that lower charge states are stable or that higher charge states are accessible. There are no reversible waves in the cyclic voltammogram of the copper complex **7**. The electrochemical data show that in comparison to complexes of the related PY5Me$_2$ ligand,[7] the PY4Im ligand stabilizes the trivalent metal oxidation state by at least 0.25 V. The large stabilization of the Ni(III) oxidation state in particular is remarkable, and is
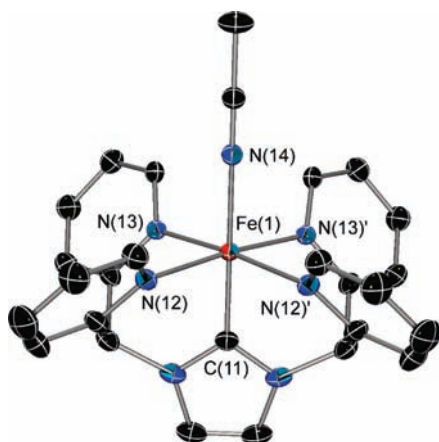
Table 2. Cyclic Voltammetry Data Showing $E_{1/2}$ for the $[(PY4Im)M(MeCN)]^{2+/3+}$ Couples of **4**−**6** in Acetonitrile [a]

M	PY4Im	PY5Me₂[b]
Fe	0.50	0.76
Co	−0.19	0.17
Ni	0.51	1.32

[a] All couples are referenced to the Cp_2Fe/Cp_2Fe^+ couple, 0.1 M NBu_4PF_6 in MeCN. [b] Data from reference 7.

Figure 7. X-ray crystal structure of $[(PY4Im)Fe(MeCN)]^{3+}$, as observed in **8**. Thermal ellipsoids are shown at 50% probability; hydrogen atoms are omitted for clarity. Selected bond lengths (Å) and angles (deg): Fe(1)−C(11) 1.889(5); Fe(1)−N(14) 1.991(4); Fe(1)−N(12) 2.026(3); Fe-(1)−N(13) 2.021(3); C(11)−Fe(1)−N(14) 179.3(2); N(13)−Fe(1)−N(12) 173.6 (1).

Scheme 4
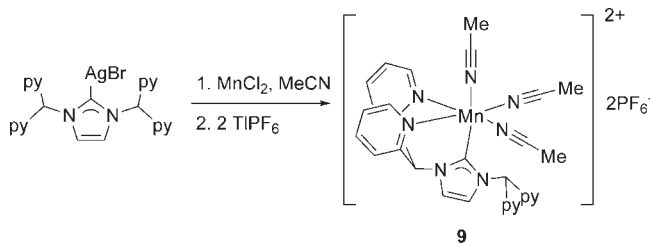
possibly related to the large difference between the ionic radii of low spin nickel(II) and nickel(III). [29] The smaller nickel(III) ion, which is similar in size to low spin iron(III), is expected to have a significantly better match for the small binding pocket of the PY4Im ligand. In summary, the electrochemical data clearly show the stronger donor ability of the PY4Im ligand, due in part to the strongly donating NHC moiety.

In the case of iron, the higher oxidation state was synthetically accessed by treating **4** with the thianthrenyl radical cation (Scheme 3). The resulting trivalent complex [(PY-4Im)Fe(MeCN)](PF₆)₃ **8** was structurally characterized by X-ray crystallography (Figure 7). The solid-state structure of **8** is similar to that of its divalent precursor **4**, with little change in the equatorial Fe−N bond lengths upon oxidation. There is a slight elongation of the Fe(1)−C(11) and Fe(1)−N(16) bond lengths, which may be due to reduced π-back-bonding from the low spin iron(III) center. As a result of the longer Fe(1)−C(11) distance, the iron atom lies slightly farther out of the Py4 ligand plane (0.111(2) Å). There is also an increase in the average $Fe-N-C-C(sp^3)$ torsion
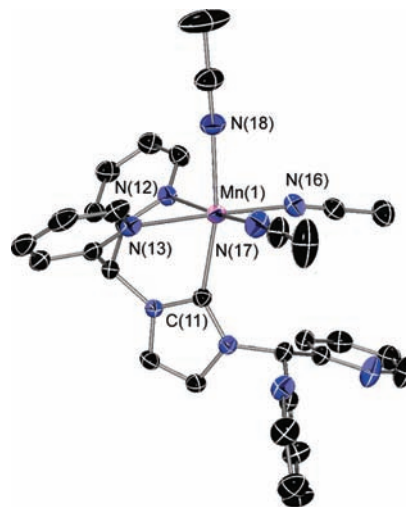
Figure 8. X-ray crystal structure of $[(\kappa^3\text{-}PY4Im)Mn(MeCN)_3]^{2+}$, as observed in **9**. Thermal ellipsoids are shown at 50% probability, hydrogen atoms omitted for clarity. Selected bond lengths (Å) and angles (deg): Mn(1)−C(11) 2.213(2); Mn(1)−N(12) 2.2625(17); Mn(1)−N(13) 2.3062(18); Mn(1)−N(16) 2.251(2); Mn(1)−N(17) 2.1917(19); Mn(1)−N-(18) 2.253(2); C(11)−Mn(1)−N(12) 84.27(7); C(11)−Mn(1)−N(13) 80.62(7); C(11)−Mn(1)−N(16) 96.22(7); C(11)−Mn(1)−N(17) 101.32(7); C(11)−Mn(1)−N(18) 167.95(7).

angle to 5.7(5) ° upon oxidation. The latter two results reinforce the hypothesis that low-spin iron(II) provides the best fit for the Py4Im ligand (Figure 6).

The solution structure of the iron(III) complex in **8** is consistent with that of the solid-state, as determined by ¹H NMR spectroscopy. Six paramagnetically shifted resonances with appropriate integrations for the PY4Im ligand are observed between 46 and −61 ppm. The magnetic moment of the complex, as measured by Evans′ method ($\mu_{eff} = 2.5\,\mu_B$) is consistent with low spin ($S = {}^1/_2$) Fe(III).

In contrast to the other transition metals reported here, the PY4Im ligand does not bind to manganese in a pentadentate fashion. Instead, reaction of **3** with $MnCl_2$, followed by anion metathesis with $TlPF_6$, results in formation of $[(\kappa^3\text{-}PY4Im)Mn(MeCN)_3](PF_6)_2$ **9** (Scheme 4). The single crystal X-ray structure of **9** shows that, in stark contrast to pentadentate binding mode observed for the later transition metals, in this complex the PY4Im ligand ligates in a tridentate, face-capping mode (Figure 8). Three acetonitrile ligands complete the coordination sphere of the manganese-(II) ion. Another striking difference with the other PY4Im complexes is the long Mn(1)−C(11) distance (2.213(2) Å), which is similar to other high-spin manganese(II) NHC complexes,[30] but over 0.2 Å longer than in **4**−**8**. Since the Mn(1)−N(12) and Mn(1)−N(13) distances are within the normal ranges for manganese(II), it is likely that the relatively long metal−carbon bond length prevents the potentially pentadentate PY4Im ligand from fully enveloping the metal center. Further evidence for this hypothesis stems from the C(11)−M(1)−N(18) bond angle, which is bent in **9** (167.95-(7)°) and linear in complexes **4**−**8**. Therefore, in the case of

(30) (a) Abernethy, C. D.; Cowley, A. H.; Jones, R. A.; Macdonald, C. L. B.; Shukla, P.; Thompson, L. K. *Organometallics* **2001**, *20*, 3629. (b) Chai, J.; Zhu, H.; Most, K.; Roesky, H. W.; Vidovic, D.; Schmidt, H.-G.; Noltemeyer, M. *Eur. J. Inorg. Chem.* **2003**, 4332. (c) Chai, J.; Zhu, H.; Peng, Y.; Roesky, H. W.; Singh, S.; Schmidt, H.-G.; Noltemeyer, M. *Eur. J. Inorg. Chem.* **2004**, 2673. (d) Pugh, D.; Wright, J. A.; Freeman, S.; Danopoulos, A. A. *Dalton Trans.* **2006**, 775.

the manganese(II) cation, the PY4Im ligand is not a sufficiently strong donor to enforce a low spin state, and does not provide a large enough binding pocket to encapsulate the relatively large ion. It is likely that either larger or more strongly donating variants of the PY4Im ligand would bind manganese(II) in a pentadentate fashion.

Conclusions

In conclusion, incorporating an axial NHC donor into a pentadentate framework has an impact on both the steric and the electronic properties of the ligand. As with related pentadentate ligands, PY4Im adopts a square pyramidal coordination mode in the series of complexes containing divalent first row metal ions from iron to copper. However, the binding pocket of the PY4Im ligand is too small to accommodate the high spin manganese(II) ion, in contrast to related pentadentate ligands. Spectral and electrochemical data provide evidence for the strongly donating nature of the ligand and its ability to stabilize trivalent metal ions, although there is no evidence that unusually high oxidation states are accessible. The synthesis of new pentadentate ligands that either incorporate multiple NHC donors or more strongly donating carbene donor(s) may ultimately prove successful in this regard.

Supporting Information Available: Crystallographic information files (CIF) for all structures, full crystallographic tables, selected metrical data, and EPR spectra of complexes **5** and **7**. This material is available free of charge via the Internet at http://pubs.acs.org.